Mol Biol Rep (2012) 39:5115–5123
DOI 10.1007/s11033-011-1307-z

Interaction of human serum albumin with 10-hydroxycamptothecin: spectroscopic and molecular modeling studies

Hui-Hui Sun · Jing Zhang · Ye-Zhong Zhang · Li-Yun Yang · Li-Li Yuan · Yi Liu

Received: 15 May 2011 / Accepted: 30 November 2011 / Published online: 9 December 2011

Abstract In this work, fluorescence spectroscopy in combination with circular dichroism spectroscopy and molecular modeling was employed to investigate the binding of 10-hydroxycamptothecin (HCPT) to human serum albumin (HSA) under simulative physiological conditions. The experiment results showed that the fluorescence quenching of HSA by HCPT was a result of the formation of HCPT–HSA complex. The corresponding association constants (K_a) between HCPT and HSA at four different temperatures were determined according to the modified Stern–Volmer equation. The results of thermodynamic parameters ΔG, ΔH, and ΔS indicated that hydrogen bonds and van der Waals forces played major roles for HCPT–HSA association. Site marker competitive displacement experiment indicated that the binding of HCPT to HSA primarily took place in sub-domain IIA (site I). Molecular docking study further confirmed the binding mode and the binding site obtained by fluorescence and site marker competitive experiments. The conformational investigation showed that the presence of HCPT decreased the α-helical content of HSA and induced the slight unfolding of the polypeptides of protein, which confirmed some micro-environmental and conformational changes of HSA molecules.

Keywords Binding site · Circular dichroism · Fluorescence spectrum · Human serum albumin · Molecular modeling · 10-Hydroxycamptothecin

H.-H. Sun · J. Zhang · Y.-Z. Zhang (✉) · L.-Y. Yang · L.-L. Yuan · Y. Liu (✉)
College of Chemistry and Environmental Engineering, Yangtze University, Jingzhou 434023, Hubei, People's Republic of China
e-mail: zhangfluorescence@126.com

Y. Liu
e-mail: prof.liuyi@263.net

Y. Liu
College of Chemistry and Molecular Sciences and State Key Laboratory of Virology, Wuhan University, Wuhan 430072, People's Republic of China

Introduction

Camptothecin (CPT) is a natural alkaloid isolated in the 1960s from extracts of camptotheca acuminate, a native plant in China. Due to the promising and potent anti-tumor activity in human neoplasms, CPT and its derivatives have received more and more attention in recent years. CPTs have potential anti-tumor activities with a novel mechanism of action, targeting the nuclear enzyme topoisomerase I (Top I) and inhibiting the relegation of the cleaved DNA strand, which leads to the death of tumor cells [1–3]. 10-hydroxycamptothecin (HCPT, the structure shown in Fig. 1), the natural CPT analogue, has shown the most strong anti-tumor effects among its analogues, and less toxic in experimental animals and in human clinical evaluations compared to CPT [4, 5]. It has been widely used in the treatment of gastric carcinoma, hepatoma, bladder carcinoma, lung cancer, colonic cancer, leukemia, and tumor of head and neck in clinical practice [6–9]. As a potential new protein targeted drug, it has been demonstrated that HCPT can bind to serum albumin in blood [10], but its effects on serum albumin remain unclear. As it is widely accepted in the pharmaceutical industry that the overall distribution, metabolism, and efficacy of many drugs can be affected based on their affinity to serum albumin. We think that the investigation of the interaction and binding affinity between HCPT and serum albumin at a

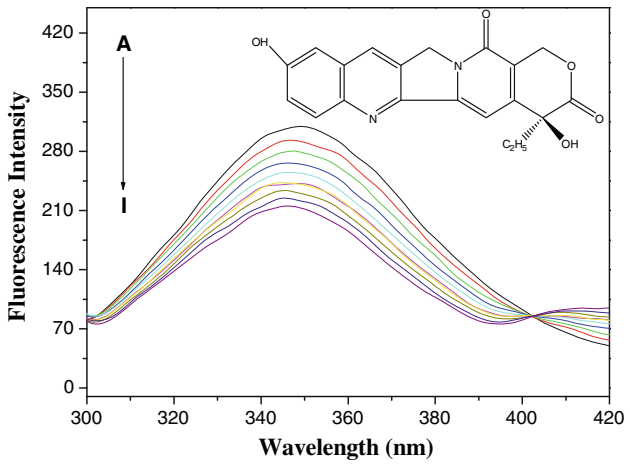

Fig. 1 Molecular structure of HCPT and emission spectra of HSA in the presence of various concentrations HCPT ($T = 298$ K, $\lambda_{ex} = 285$ nm. c(HSA) = 2.0×10^{-6}mol L^{-1}; c(HCPT)/(10^{-6} mol L^{-1}), A–I: 0, 0.5, 1.0, 1.5, 2.0, 2.5, 3.0, 3.5, 4.0, respectively

molecular level can provide important clues for understanding the pharmacokinetics and pharmacodynamic properties of HCPT.

Human serum albumin (HSA) is the principal extracellular protein of the circulatory system, and accounts for about 60% of the total plasma proteins corresponding to a concentration of 42 mg/ml [11, 12]. In addition, HSA plays key roles in the transport, distribution, and metabolism of many endogenous and exogenous ligands, such as fatty acids, steroid hormones, metabolites, and an extraordinarily broad range of drugs [13]. And thus, HSA has been frequently selected as the model protein for investigating the protein folding and drug-binding mechanism [14].

Recently, extensive researches about the interaction between HSA and internal compound or pharmaceutical molecules have been reported [15–18], but interactions of HSA with CPT and their derivatives have seldom been investigated. The present work is to investigate the interaction between HCPT and HSA by fluorescence spectroscopy, circular dichroism (CD) spectroscopy and molecular modeling method. Great attempts have been made to investigate the interaction mechanism between them regarding the quenching mechanism, the specific binding site, the type of interaction force, and the effect of HCPT on the micro-environmental and conformational changes of HSA molecules.

Experimental

Materials

HSA (electrophoresis grade reagents) was purchased from Sigma Aldrich (St. Louis, MO, USA) and used without further purification. The HSA working solutions were prepared to be the concentration of 2.0×10^{-6} mol l^{-1} in Tris-HCl buffer solutions (0.10 mol l^{-1} Tris base, 0.10 mol l^{-1} HCl and 0.10 mol l^{-1} NaCl, pH 7.40) and stored in the dark prior to use. HCPT was purchased from NICPBP (National Institute for the Control of Pharmaceutical and Biological Products). The stock solutions of HCPT were prepared with the concentration of 5.0×10^{-4} mol l^{-1} in 0.10 mol l^{-1} NaOH solution. All other reagents and solvents were of analytical purity and doubly distilled water was used throughout the experiment. The weight measurements were performed with an AY–120 electronic analytic weighting scale (Shimadzu, Japan) with a resolution of 0.1 mg. SYC-15 super constant temperature water bath (Nanjing Sangli Electronic Equipment Factory, temperature control accuracy ± 0.1°C) was used to control the temperature of fluorescence experiments.

Equipment and methods

All fluorescence data were performed on an LS–55 Spectrofluorimeter (Perkin-Elmer corporate, America) equipped with 1.0 cm quartz cells and a thermostat bath. Fluorescence emission spectra were recorded at four different temperatures (292, 298, 304 and 310 K) in the range of 300–450 nm. The widths of the excitation and emission slit were set to 15.0 and 4.0 nm, respectively. An excitation wavelength of 285 nm was chosen and the temperature of sample was kept by the recycle water in the experiment. All titrations were done manually by trace syringes.

Site marker competitive experiments

Binding studies between HCPT and HSA in the presence of two site markers (Warfarin and Ibuprofen) were measured using the fluorescence titration methods. The concentrations of HSA and site markers were held in equimolar concentration, HCPT was then gradually added to the HSA–Warfarin or HSA–Ibuprofen mixtures. An excitation wavelength of 285 nm was selected and the fluorescence spectra were recorded in the range of 300–450 nm.

Molecular modeling

The crystal structure of the HSA was from PDB database. The structure of HSA was analyzed with sybyl8.1 software. All the ligands and water molecules were removed before the analysis. H atoms were added and the biopolymer was charged using AMBER7 FF99 method. The structure of HCPT was generated with sybyl8.1 package and the molecule was energy minimized using Tripos Force Field, after been charged with Gasteiger and Marsili method. The PDB entry of the HSA crystal structure employed in docking

study was 1H9Z. Docking study was conducted by a Surflex-Dock program in Sybyl 8.1 package.

CD measurements were performed on a J-810 Spectropolarimeter (Jasco, Tokyo, Japan) at room temperature (pH = 7.4). The CD measurements of HSA in the absence and presence of HCPT (1:0, 1:2, 1:6) were recorded in the range of 260–200 nm. The instrument was controlled by Jasco's Spectra Manage™ software. Quartz cells having path lengths of 0.1 cm were used at a scanning speed of 200 nm/min. The data were expressed in terms of mean residue ellipticity (MRE). Appropriate buffer solution running under the same conditions was taken as blank and subtracted from the sample spectra.

The 3-dimensional fluorescence spectra were performed under the following conditions: the emission wavelength was recorded between 200 and 500 nm, the initial excitation wavelength was 200 nm with an increment of 5 nm, the number of scanning curves was 31, and other scanning parameters were the same as those of the fluorescence quenching spectra.

Results and discussions

Fluorescence quenching mechanism and quenching constant

Fluorescence quenching refers to any process that decreases the fluorescence intensity of a fluorophore. The different mechanisms of quenching are usually classified as either dynamic quenching or static quenching and they can be distinguished by their different dependence on temperature or viscosity, or by lifetime measurements [19, 20]. Higher temperatures can result in faster diffusion and then higher dynamic quenching constants. In contrast, increasing of temperature results in decreased stability of complexes, thus the values of the static quenching constants are expected to be smaller [21].

In the present work, the fluorescence quenching spectra of HSA in the presence of different concentrations of HCPT at four different temperatures (292, 298, 304, and 310 K) were measured to elucidate the quenching mechanism. The effect of HCPT on the fluorescence intensity of HSA at 298 K is depicted in Fig. 1. Obviously, HSA has a strong fluorescence emission band at 350 nm when excited at 285 nm, which was mainly due to the fluorescence emission of tryptophan residues. When different amount of HCPT was added to a fixed concentration of HSA, a gradually decrease in the fluorescence intensity of HSA was observed, indicating that HCPT could interact with HSA and quench its intrinsic fluorescence. The fluorescence quenching was usually analyzed using the well-known Stern–Volmer equation [22]:

$$\frac{F_0}{F} = 1 + K_{SV}[Q] = 1 + k_q\tau_0[Q] \quad (1)$$

where F_0 and F denote the steady-state fluorescence intensities in the absence and presence of quencher (HCPT), respectively. K_{SV} is the Stern–Volmer quenching constant and [Q] is the concentration of quencher. k_q is the quenching rate constant of the biological macromolecule and k_q is equal to K_{SV}/τ_0. τ_0 is the average lifetime of the molecule without any quencher and the fluorescence lifetime of the biopolymer is 10^{-8} s [23]. The Stern–Volmer plots for the HCPT–HSA system at four different temperatures are shown in Fig. 2a. Accordingly, Eq. 1 was applied to determine K_{SV} by linear regression of a plot of F_0/F against [Q]. The calculated quenching constants K_{SV} and k_q at corresponding temperatures are summarized in Table 1. The results show that K_{SV} is inversely correlated with temperature and k_q is much greater than 2.0×10^{10} l mol^{-1} s^{-1}, which indicate that the

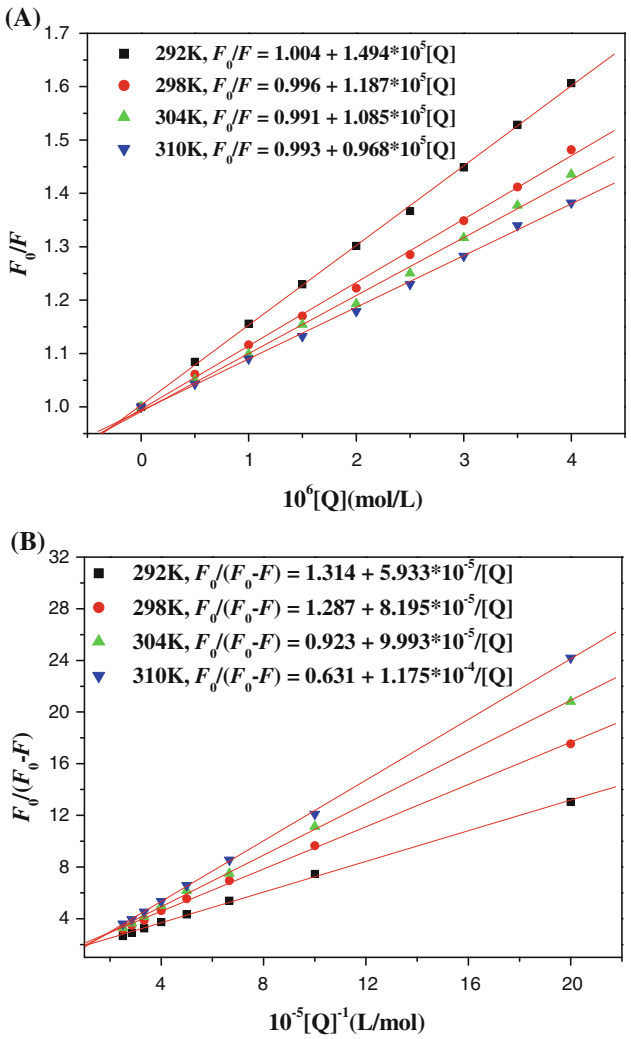

Fig. 2 Stern–Volmer plots (**a**) and modified Stern–Volmer plots (**b**) for the HCPT–HSA system at four different temperatures, pH 7.4

Table 1 Stern–Volmer quenching constants for the interaction of HCPT with HSA at four different temperatures

pH	T (K)	K_{SV} ($\times 10^5$ l mol^{-1})	K_q ($\times 10^{13}$ M^{-1} S^{-1})	R^a
7.4	292	1.494 ± 0.034	1.494 ± 0.034	0.9997
	298	1.187 ± 0.032	1.187 ± 0.032	0.9991
	304	1.085 ± 0.019	1.085 ± 0.019	0.9982
	310	0.993 ± 0.044	0.993 ± 0.044	0.9991

[a] R is the correlation coefficient

fluorescence quenching of HSA was probably induced by the formation of a HCPT–HSA complex rather than by dynamic collision [24]. The occurrence of an isoactinic point at 402 nm might also indicate the existence of bound and free HCPT in equilibrium [25].

Therefore, the fluorescence quenching of HSA by HCPT should be analyzed using the modified Stern–Volmer equation [26]:

$$\frac{F_0}{\Delta F} = \frac{1}{f_a K_a}\frac{1}{[Q]} + \frac{1}{f_a} \quad (2)$$

In the present case, K_a is the effective quenching constant for the accessible fluorophores, f_a is the fraction of accessible fluorescence. Figure 2b displays the modified Stern–Volmer plots, and the corresponding values of K_a at different temperatures are listed in Table 2. The decreasing trend of K_a with increasing temperature is in accordance with K_{SV}'s dependence on temperature, which coincides with the static quenching mechanism [20].

Thermodynamic parameters and type of binding forces

Generally, the interaction forces between small organic molecules and biological macromolecules may include hydrophobic force, hydrogen bond, van der Waals force and electrostatic interactions, etc. Ross and Subramanian [27] have characterized the signs and magnitudes of the thermodynamic parameters associated with various kinds of interaction force that may take place in protein association process. Considering the dependence of the binding constant (HCPT–HSA) on temperature, a thermodynamic process was considered to be responsible for the formation of the complex. Thermodynamic parameters for a binding interaction can be used as major evidence for the nature of intermolecular forces. The enthalpy (ΔH) of the reaction of HCPT and HSA can be treated as a constant in case there is no remarkable change on temperature and the thermodynamic parameters can be calculated from the Van't Hoff equation [28]:

$$\ln K = -\frac{\Delta H}{RT} + \frac{\Delta S}{R} \quad (3)$$

$$\Delta G = \Delta H - T\Delta S = -RT \ln K \quad (4)$$

where K corresponds to the effective binding constant K_a and R is the gas constant. The value of ΔH and ΔS can be calculated from the slope and intercept of the plot of ln$K$ versus $1/T$. The value of ΔG was obtained according to Eq. 4. All the values above were summarized in Table 2. It was observed that the formation of the HSA–HCPT complex was a spontaneous process with a negative value of ΔG. We can see that the binding reaction of HCPT to HSA is exothermic ($\Delta H < 0$). This means that higher temperatures should weaken the binding, which is also shown by the decreasing values of K_a in Table 2. An important source of negative contribution to ΔH and ΔS will arise if a hydrogen bond is formed. Therefore, the negative ΔH and ΔS values, show that both hydrogen bonds and van der Waals forces play a role in the binding of HCPT to HSA, which complies with the multihydroxyl and multicarbonyl structure of HCPT [29].

Site-selective binding of HCPT on HSA

In order to identify the HCPT-binding site on HSA, some probes are often used, which specifically bind to a known site or region on HSA. From X-ray crystallography studies, Warfarin has been demonstrated to bind to the sub-domain IIA (site I) while Ibuprofen is considered as sub-domain IIIA (site II) binder [30]. In order to identify the binding site of HCPT on HSA, site marker competitive experiment was carried out, using drugs (warfarin and ibuprofen) which specifically bind to known sites or regions on HSA. Then

Table 2 Modified Stern–Volmer association constants K_a and relative thermodynamic parameters of the HCPT–HSA system

T (K)	K_a ($\times 10^5$ l mol^{-1})	R^a	ΔH (kJ mol^{-1})	ΔG (kJ mol^{-1})	ΔS (J mol^{-1} K^{-1})	R^b
292	2.214 ± 0.012	0.9993	−59.85 ± 0.60	−29.01 ± 0.34	−102.1 ± 1.9	0.9932
298	1.571 ± 0.016	0.9995				
304	0.923 ± 0.012	0.9996				
310	0.537 ± 0.015	0.9999				

[a] R is the correlation coefficient for the K_a values

[b] R is the correlation coefficient for the van't Hoff plot

information about the binding site can be gained by monitoring the changes in the fluorescence of HCPT bound HSA that brought about by site I (warfarin) and site II (ibuprofen) markers. In the site marker competitive experiment, HCPT was gradually added to the solution of HSA with site markers held in equimolar concentrations (2.0×10^{-6} mol l^{-1}). With the addition of ibuprofen into the HSA solution, the fluorescence property of the HCPT–HSA system was almost the same as that of without ibuprofen (Fig. 3b), which suggested that ibuprofen did not prevent the binding of HCPT in its usual binding location. By contrast, the addition of warfarin into HSA solution resulted in the slightly red shift of the maximum emission wavelength of HSA and the significantly decrease of the fluorescence intensity (Fig. 3a). Then, with the continuing addition of HCPT into the above system, the fluorescence intensity of HSA decreased gradually and the

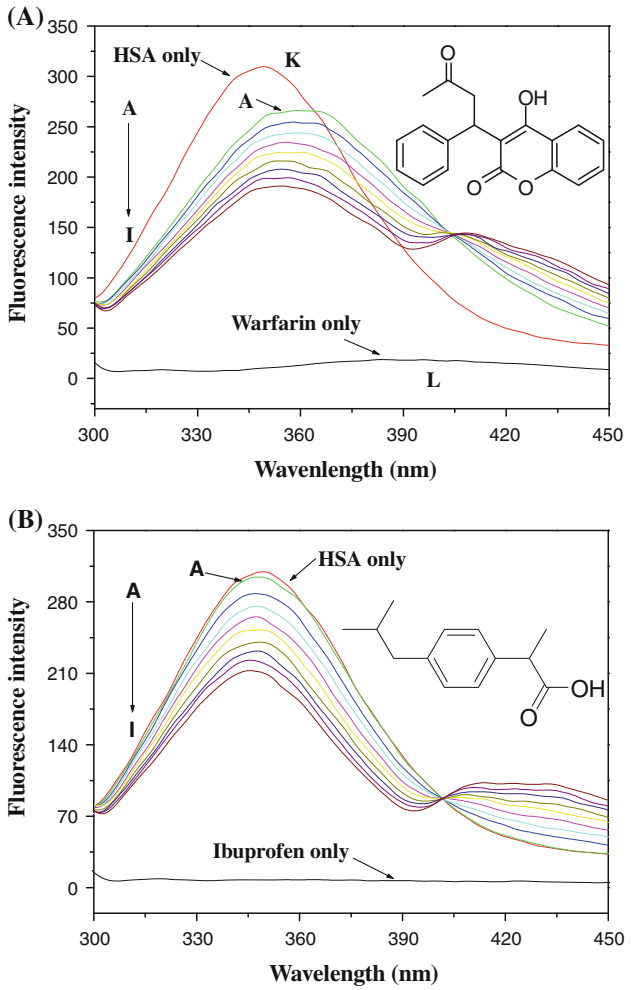

Fig. 3 Effect of selected site markers on the fluorescence of HCPT bound HSA ($T = 298$ K, $\lambda_{ex} = 285$ nm). (**a**) c(HSA) = c(Warfarin) = 2.0×10^{-6} mol L^{-1}; (**b**) c(HSA) = c(Ibuprofen) = 2.0×10^{-6} mol L^{-1}; c(HCPT)/(10^{-6} mol L^{-1}), A–I: 0, 0.5, 1.0, 1.5, 2.0, 2.5, 3.0, 3.5, 4.0, respectively. The inserts correspond to the molecular structures of site markers

Table 3 The modified Stern–Volmer association constants of competitive experiments for HCPT–HSA system at room temperature (at 298 K)

Site marker	K_a ($\times10^5$ l mol^{-1})	R^a
Blank	1.571 ± 0.013	0.9995
Ibuprofen	1.409 ± 0.067	0.9992
Warfarin	0.991 ± 0.10	0.9994

[a] R is the correlation coefficient

intensity was much lower than that of without warfarin. This indicated an increased polarity of the region surrounding the tryptophan site (Trp-214) and an obviously affection of the bound HCPT to HSA by the adding warfarin. To facilitate the comparison of the influence of warfarin and ibuprofen on the binding of HCPT to HSA, the binding constants with the presence of site markers were analyzed using the modified Stern–Volmer equation (Eq. 2). The binding constants of the systems, which can be calculated from the slope values of the plots, were listed in Table 3. Obviously, the binding constant of the system with warfarin was almost 63.1% of that without warfarin, while the constants of the systems with and without ibuprofen had only a small difference, indicating that warfarin could significantly affect the binding of HCPT to HSA, while ibuprofen had only a small influence. The above experimental results and analysis demonstrated that the decrease in HSA fluorescence was resulted from the competitive displacement of the probe, and the binding of HCPT to HSA mainly located within site I (sub-domain IIA).

Molecular modeling

The crystallographic analyses of HSA have showed that the protein, a 585 amino acid residues monomer, contains three homologous α-helical domains (I–III): I (residues 1–195), II (residues 196–383), III (residues 384–585), and each containing two subdomains (A and B) [31]. HSA has a limited number of binding sites for endogenous and exogenous ligands that are typically bound reversibly and have binding constants in the range 10^4–10^8 M^{-1} [32]. The principal regions of ligand binding sites of albumin are located in hydrophobic cavities in subdomains IIA and IIIA, which are consistent with sites I and II, respectively, and one tryptophan residue of HSA is in subdomain IIA. There is a large hydrophobic cavity present in subdomain IIA that many drugs can bind [33]. The application of molecular modeling by computer method has been employed to improve the understanding of the interaction of HCPT and HSA. The Sybyl 8.1 program was chosen to examine the binding mode of HCPT at the active site of HSA. The 3-D structure of HSA was obtained from Proteins Data Bank database. The initial structures of all the molecules were generated by molecular modeling software

Sybyl8.1. The geometries of HCPT were subsequently optimized using the Tripos force field with Gasteiger–Marsili charges. Suflex-dock program was applied to calculate the possible conformation of HCPT that binds to HSA. Suflex-dock program was used to build the interaction modes between the HCPT and HSA. HCPT was docked to HSA by Suflex-dock program and then it revealed hydrogen bonds (yellow dashed line in Fig. 4b, c) between HCPT and some residues of HSA [34].

As shown in Fig. 4, HCPT was located within the binding pocket of subdomain IIA in site I formed by helices and site I was large enough to accommodate the HCPT molecule, and it was important to note that HCPT was adjacent to polar amino acid residues with positive charges: Arg-257, Arg-218, Arg-222, His-288, Lys-195, etc., of subdomain IIA of HSA. Furthermore, there are a number of hydrogen bonds formed between HCPT and Arg-257, Arg-218, Arg-222, His-288 of HSA (there are seven hydrogen bonds indicated by yellow dashed line). Therefore, the results obtained from molecular modeling indicate that the interaction between HCPT and HSA is dominated by hydrogen bonds and van der Waals forces, the formation of hydrogen bonds increasing the stability of the HCPT–HSA system, which is in good agreement with the result of the binding mode. The proofs coming from molecular modeling also suggested that HCPT can bind to HSA at site I in subdomain IIA, which is in accordance with the site marker competitive study.

Conformational investigations

When drugs interacted with HSA, the intramolecular forces that responsible for maintaining the secondary or tertiary structures of protein can be affected, which may further result in a conformational change of protein. To get insight of the structural changes of HSA induced by HCPT binding, the CD and 3-dimensional fluorescence spectra of HSA were measured.

CD spectrum has been demonstrated to be a sensitive technique in monitoring the secondary structural change of protein upon interaction with drugs. The CD spectra of HSA exhibits two negative bands at 208 and 222 nm, characteristic of the typical α-helix structure of protein [35]. The reasonable explanation is that the negative peaks of 208–209 and 222–223 nm were contributed to the n $\rightarrow$ π^* transfer for the peptide bond of α-helixes. The CD spectra of HSA with various concentrations of HCPT at pH 7.4 and room temperature are shown in Fig. 5. It can be seen that the relative band intensity of curves A to C decreased regularly with the increasing addition of HCPT, suggesting the change of the protein secondary structure. This might be induced by the formation of the HCPT–HSA complex.

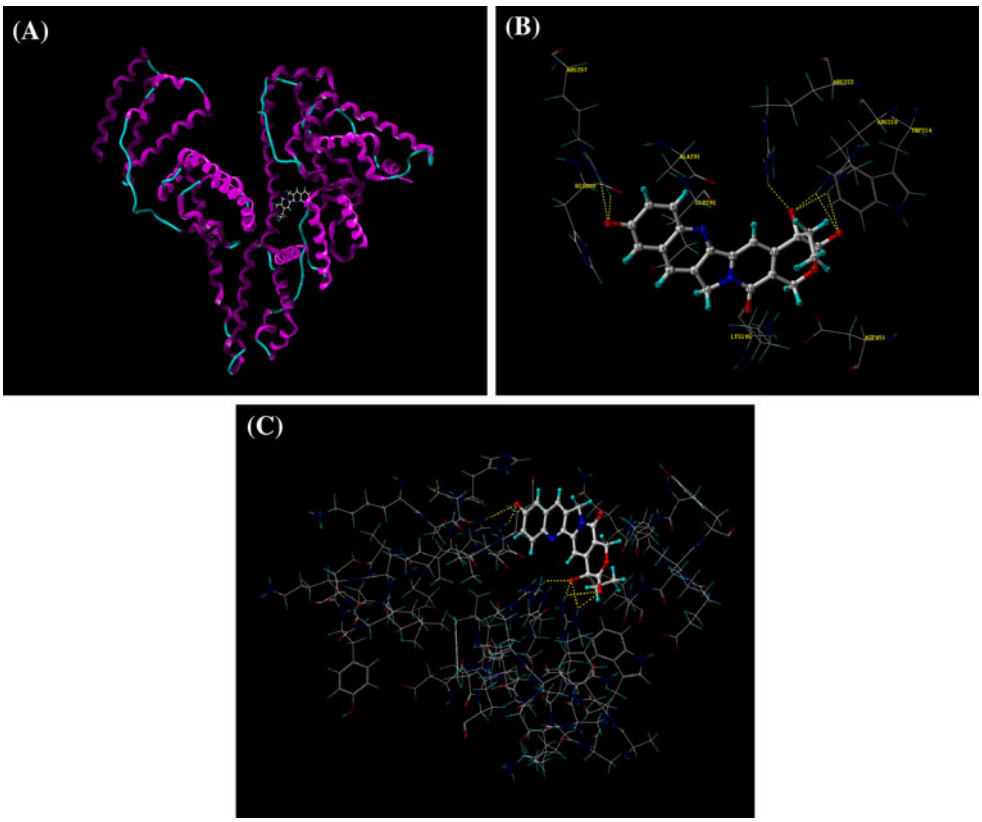

Fig. 4 Molecular modeling of HCPT bound HSA. The residues of HSA and HCPT are represented using different tinctorial stick model. (**a**) Binding site of HCPT in HSA. (**b**) (**c**) Conformation of HCPT in the binding site of HSA. The hydrogen bond between the ligand and the protein is indicated by yellow dashed line. (Color figure online)

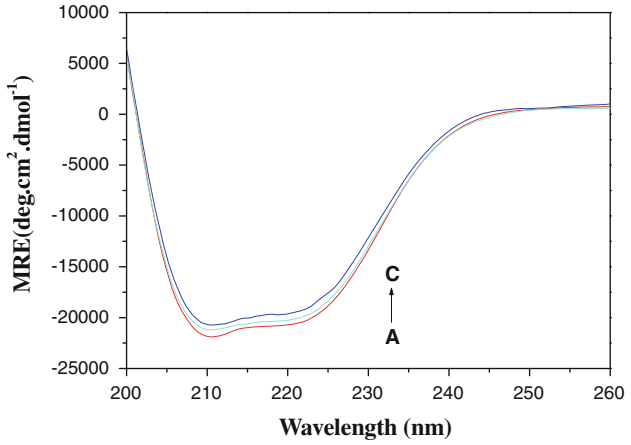

Fig. 5 The CD spectra of the HCPT–HSA system obtained at room temperature and pH 7.4; c(HSA) = 2.0×10^{-6}mol L^{-1}; c(HCPT)/(10^{-6}mol L^{-1}), A–C: 0, 4.0, 12.0, respectively

However, the shape of peaks and the peak maximum position remained almost unchanged in the presence and absence of HCPT, indicating that the HSA has predominantly α-helix nature even after binding to the drug.

In order to quantify the content of different secondary structure of HSA, the algorithm SELCON3 was applied to analyze the CD spectra, using 43 mode proteins with known precise secondary structures as the reference set [36, 37]. The fraction contents of different secondary structures of HSA in the absence and presence of HCPT are listed in Table 4. A decreasing tendency of the α-helix content (from 60.0 to 57.3%) and an increasing tendency of β-strands, turn, and unordered structure contents were observed with the increasing concentration of HCPT. This revealed that the polypeptides of HSA had alternatively unfolded and the secondary structure had been potential perturbation at high drug concentrations, which is important for biomedical applications [38].

Table 4 Fractions of different secondary structures determined by SELCON3

Molar ratio [HCPT]:[HSA]	H(r) (%)	H(d) (%)	S(r) (%)	S(d) (%)	Trn (%)	Unrd (%)
0:1	40.3	19.7	3.0	3.0	13.0	21.0
2:1	39.1	19.6	3.3	3.3	13.6	21.1
6:1	37.8	19.5	3.4	3.6	14.3	21.4

H(r) regular α-helix, *H(d)* distorted α-helix, *S(r)* regular β-strand, *S(d)* distorted β-strand, *Trn* turns, *Unrd* unordered structure

3-Dimensional fluorescence spectrum (3-D FL), which can comprehensively exhibit the fluorescence information of the chromophore and make the investigation of the characteristic conformational change of protein be more scientific, was applied in the present work. The 3-D FL of HSA and HCPT–HSA system are shown in Fig. 6, and the corresponding characteristic parameters are listed in Table 5. By comparing the spectral changes of HSA in the absence and presence of HCPT, the conformational and micro-environmental changes of HSA can be obtained. As shown in Fig. 6, peak *a* is the Rayleigh scattering peak ($\lambda_{ex} = \lambda_{em}$), peak *b* is the second-ordered scattering peak ($\lambda_{em} = 2\lambda_{ex}$).The fluorescence intensity of peak *a* increased with the addition of HCPT, and the reasonable explanation is that a HCPT–HSA complex came into being after the addition of HCPT, making the diameter of the macromolecule increased, which in turn resulted in the enhancement of the scattering effect [39].

Peak 1 ($\lambda_{ex} = 285.0$ nm, $\lambda_{em} = 348.5$ nm) mainly reveals the spectral behavior of tryptophan and tyrosine residues, the maximum emission wavelength and the fluorescence intensity of the residues are in close correlation with the polarity of the microenvironment [40]. Besides peak 1, there is another strong fluorescence peak (peak 2, $\lambda_{ex} = 230.0$ nm, $\lambda_{em} = 347.5$ nm) that mainly exhibits the fluorescence characteristic of polypeptide backbone structures C=O of HSA and the fluorescence intensity of this peak is correlated with the secondary structure of protein [41]. As shown in Fig. 6, the fluorescence intensity of peak 2 decreased obviously (from 305.9 to 243.7) after the addition of HCPT, which indicated that the interaction of HCPT with HSA induced the unfolding of the polypeptides

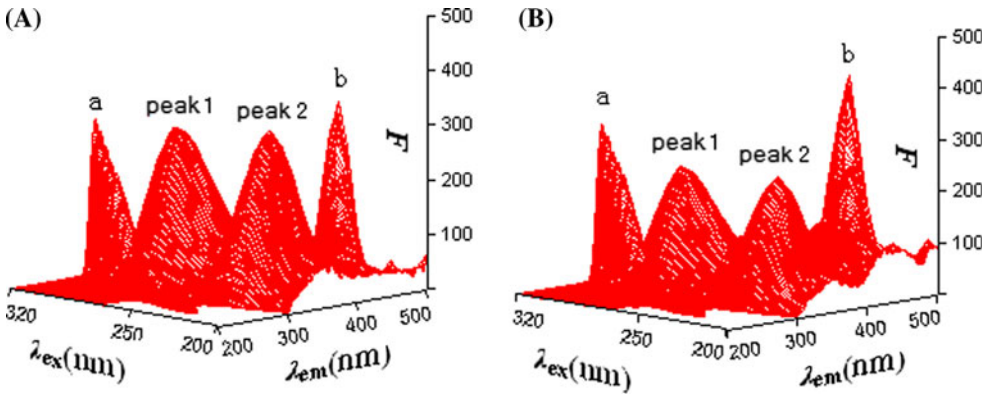

Fig. 6 Three-dimensional fluorescence spectra of HSA (**a**) and HCPT–HSA system (**b**), c(HSA)/(10^{-6} mol L^{-1}), A: 2.0, B: 2.0; c(HCPT)/(10^{-6} mol L^{-1}) A: 0, B: 2.0

Table 5 Three-dimensional fluorescence spectral characteristics of HSA and HCPT-HSA system

Peaks	HSA			HCPT-HSA		
	Peak position $\lambda_{ex}/\lambda_{em}$ (nm/nm)	Stokes shift $\Delta\lambda$ (nm)	Intensity F	Peak position $\lambda_{ex}/\lambda_{em}$ (nm/nm)	Stokes shift $\Delta\lambda$ (nm)	Intensity F
Rayleigh scattering peaks	285/285 → 350/350	0	78.5 → 300.0	280/280 → 320/320	0	82.2 → 328.1
Fluorescence peak 1	285.0/348.5	63.5	280.9	285.0/346.5	61.5	235.0
Fluorescence peak 2	230.0/347.5.0	117.5	305.9	230.0/347.5	117.5	243.7

and conformational change of HSA. Analyzing from the fluorescence intensity changes of peak 1 and peak 2 (the intensity values were listed in Table 5), they both decreased obviously but to different degrees: the fluorescence intensity of peak 1 has been quenched of 16.3% while peak 2 of 20.3%. In combination with the decrease of the fluorescence intensity of the two peaks and the CD experimental results, it can be concluded that the interaction of HCPT with HSA induced the slight unfolding of the polypeptides of protein, which further resulted in a conformational change of the protein that increased the exposure of some hydrophobic regions which were previously buried [42]. All these phenomenon and analyses of peak 1 and peak 2 revealed that the binding of HCPT to HSA induced some micro-environmental and conformational changes in HSA.

Conclusion

The present work provided an approach for studying the interaction of HCPT with HSA by employing spectroscopic methods, CD spectroscopy and molecular modeling. It demonstrated that the fluorescence quenching of HSA was mainly induced by a static quenching mechanism and both hydrogen bonds and van der Waals forces played a major role in stabilizing the HCPT–HSA complex. The site marker competitive experiment revealed that the binding site of HCPT on HSA was located in site I (sub-domain IIA). These are also in agreement with molecular modeling results. Results from the CD and 3-D FL investigation demonstrated that the binding of HCPT to HSA resulted in some extent of conformational and micro-environmental changes of HSA.

Acknowledgments We gratefully acknowledge the financial support from National Natural Science Foundation of China (Grant No. 20921062), Research Program of Hubei Province Department of Education (D20101302) and the National Innovation Experiment Program for University Students (101048902).

References

1. Wall ME, Wani MC, Cook CE, Palmer KH, McPhail HT, Sim GA (1966) Plant antitumor agents. I. The isolation and structure of camptothecin, a novel alkaloidal leukemia and structure of camptotheca acuminata. J Am Chem Soc 88(16):3888–3890. doi:10.1021/ja00968a057
2. Dong GQ, Sheng CQ, Wang SZ et al (2010) Selection of evodiamine as a novel topoisomerase I inhibitor by structure-based virtual screening and hit optimization of evodiamine derivatives as antitumor agents. J Med Chem 53:7521–7531. doi:10.1021/jm100387d
3. Dancey J, EIsenhauer EA (1996) Current perspectives on camptothecin in cancer treatment. Br J Cancer 74:327–338. doi:10.1038/bjc.1996.362
4. Wen Y, Fan Y, Zhang M, Feng YQ (2005) Determination of camptothecin and 10-hydroxycamptothecin in human plasma using polymer monolithic in-tube solid phase microextraction combined with high-performance liquid chromatography. Anal Bioanal Chem 382:204–210. doi:10.1007/s00216-005-3194-4
5. Leu YL, Chen CS, Wu YJ, Chern JW (2008) Benzyl ether-linked glucuronide derivative of 10-hydroxycamptothecin designed for selective camptothecin-based anticancer therapy. J Med Chem 51(6):1740–1746. doi:10.1021/jm701151c
6. Hong MH, Zhu SJ, Jiang YY, Tang GT, Pei YY (2009) Efficient tumor targeting of hydroxycamptothecin loaded PEGylated niosomes modified with transferring. J Control Release 133:96–102. doi:10.1016/j.jconrel.2008.09.005
7. Lu B, Zhang ZQ (2006) Hydroxycamptothecin induced apoptosis in 5637 cells line: an in vitro model for high-risk superficial bladder cancer. J Pharm Sci 95(12):2619–2630. doi:10.1002/jps
8. Hong MH, Zhu SJ, Jiang YY, Tang GT, Pei YY (2010) Novel anti-tumor strategy: PEG-hydroxycamptothecin conjugate loaded transferrin-PEG-nanoparticles. J Control Release 141:22–29. doi:10.1016/j.jconrel.2009.08.024
9. Zhang LY, Yang M, Wang Q, Li Y, Guo R, Jiang XQ, Yang CZ, Liu BR (2007) 10-Hydroxycamptothecin loaded nanoparticles: preparation and antitumor activity in mice. J Control Release 119:153–162. doi:10.1016/j.jconrel.2007.02.013
10. Yang L, Cui FD, Cun DM, Tao AJ, Shi K, Lin WH (2007) Preparation, characterization and biodistribution of the lacton form of 10-hydroxycamptothecin (HCPT)-loaded bovine serum albumin (BSA) nanoparticles. Int J Pharm 340:163–172. doi:10.1016/j.ijpharm.2007.03.028
11. Nehal I, Hany I, Sothea K, Jean-Pierre N, Francoise N (2010) Interactions between antimalarial indolone-*N*-oxide derivatives and human serum albumin. Biomacromolecules 11:3341–3351. doi:10.1021/bm100814n
12. Ding F, Liu W, Zhang L, Yin B, Sun Y (2010) Sulfometuron-methyl binding to human serum albumin: evidence that sulfometuron-methyl binds at the Sudlow's site I. J Mol Struct 968:59–66. doi:10.1016/j.molstruc.2010.01.020
13. Cao H, Chen LS, Xiao JB (2011) Binding citrus flavanones to human serum albumin: effect of structure on affinity. Mol Biol Rep 38:2257–2262. doi:10.1007/s11033-010-0356-z
14. Froehlich E, Mandeville JS, Jennings CJ, Sedaghat-Herati R, Tajmir-Riahi HA (2009) Dendrimers bind human serum albumin. J Phys Chem B 113:6986–6993. doi:10.1021/jp9011119
15. Qin C, Xie MX, Liu Y (2007) Characterization of the myricetin-human serum albumin complex by spectroscopic and molecular

modeling approaches. Biomacromolecules 8:2182–2189. doi:10.1021/bm070319c
16. Hu YJ, Liu Y, Xiao XH (2009) Investigation of the interaction between berberine and human serum albumin. Biomacromolecules 10:517–521. doi:10.1021/bm801120k
17. Bhattacharya B, Nakka S, Guruprasad L, Samanta A (2009) Interaction of bovine serum albumin with dipolar molecules: fluorescence and molecular docking studies. J Phys Chem B 113:2143–2150. doi:10.1021/jp808611b
18. Ding F, Liu W, Diao JX, Sun Y (2011) Characterization of Alizarin Red S binding sites and structural changes on human serum albumin: a biophysical study. J Hazard Mater 186:352–359. doi:10.1016/j.jhazmat.2010.11.002
19. Hu YJ, Ou-Yang Y, Dai CM, Liu Yi, Xiao XH (2010) Binding of berberine to bovine serum albumin: spectroscopic approach. Mol Biol Rep 37:3827–3832. doi:10.1007/s11033-010-0038-x
20. Lakowicz JR (2006) Principles of fluorescence spectroscopy, 3rd edn. Springer, New York, pp 277–285
21. Zhang HX, Gao S, Xiong ZY, Liu SP (2009) Fluorometric probing on the binding of hematoxylin to serum albumin. Mol Biol Rep 36:2299–2306. doi:10.1007/s11033-009-9448-z
22. Zhang HX, Mei P (2009) In vitro binding of furadan to bovine serum albumin. J Solut Chem 38:351–361. doi:10.1007/s10953-009-9371-x
23. Kathiravan A, Renganathan R, Anandan S (2009) Interaction of colloidal $AgTiO_2$ nanoparticles with bovine serum albumin. Polyhedron 28:157–161. doi:10.1016/j.poly.2008.09.023
24. Pinto MD, Duque AL, Macias P (2010) Fluorescence spectroscopic study on the interaction of resveratrol with lipoxygenase. J Mol Struct 980:143–148. doi:10.1016/j.molstruc.2010.07.006
25. Zhang YZ, Dai J, Xiang X, Li WW, Liu Y (2010) Studies on the interaction between benzidine and bovine serum albumin by spectroscopic methods. Mol Biol Rep 37:1541–1549. doi:10.1007/s11033-009-9555-x
26. Naik P, Chimatadar SA, Nandibewoor ST (2010) Interaction between a potent corticosteroid drug—dexamethasone with bovine serum albumin and human serum albumin: a fluorescence quenching and fourier transformation infrared spectroscopy study. J Photochem Photobiol B 100:147–159. doi:10.1016/j.jphotobiol.2010.05.014
27. Ross DP, Subramanian S (1981) Thermodynamics of protein association reactions: forces contributing to stability. Biochemistry 20:3096–3102. doi:10.1021/bi00514a017
28. Katrahalli U, Jaldappagari S, Kalanur SS (2010) Study of the interaction between fluoxetine hydrochloride and bovine serum albumin in the imitated physiological conditions by multi-spectroscopic methods. J Lumin 130:211–216. doi:10.1016/j.jlumin.2009.07.033
29. Mallick A, Haldar B, Chattopadhyay N (2005) Spectroscopic investigation on the interaction of ICT probe 3-acetyl-4-oxo-6,7-dihydro-12H indolo-[2,3-a]quinolizine with serum albumins. J Phys Chem B 109:14683–14690. doi:10.1021/jp051367z
30. Hu YJ, Ou-Yang Y, Dai CM, Liu Y, Xiao XH (2010) Site-selective binding of human serum albumin by palmatine: pectroscopic approach. Biomacromolecules 11:106–112. doi:10.1021/bm900961e
31. Sjoholm I, Ekman B, Kober A, Ljungstedt-Pahlman I, Seiving B, Sjodin T (1979) Binding of drug to human serum albumin: XI. The specificity of three binding sites as studied with albumin immobilized in microparticles. Mol Pharmacol 16:767–777
32. Peters T (1996) All about albumin: biochemistry, genetics and medical applications. Academic Press, San Diego
33. Carter DC, He XM, Munson SH, Twigg PD, Gernert KM, Broom MB, Miller TY (1989) Three-dimensional structure of human serum albumin. Science 244:1195–1196
34. Li YS, Ge YS, Zhang Y, Zhang AQ, Sun SF, Jiang FL, Liu Y (2010) Interaction of coomassie brilliant blue G250 with human serum albumin: probing of the binding mechanism and binding site by spectroscopic and molecular modeling methods. J Mol Struct 968:24–31. doi:10.1016/j.molstruc.2010.01.015
35. Liu JQ, Tian JN, Tian X, Hu ZD, Chen XG (2004) Interaction of isofraxidin with human serum albumin. Bioorg Med Chem 12:469–474. doi:10.1016/j.bmc.2003.10.030
36. Bhattacharya M, Jain N, Mukhopadhyay S (2011) Insights into the mechanism of aggregation and fibril formation from bovine serum albumin. J Phys Chem B 115:4195–4205. doi:10.1021/jp111528c
37. Whitmore L, Wallace BA (2004) DICHROWEB, an online server for protein secondary structure analyses from circular dichroism spectroscopic data. Nucleic Acids Res 32:668–673. doi:10.1093/nar/gkh371
38. Brandes N, Welzel PB, Werner C, Kroh LW (2006) Adsorption-induced conformational changes of proteins onto ceramic particles: differential scanning calorimetry and FTIR analysis. J Colloid Interface Sci 299:56–69. doi:10.1016/j.jcis.2006.01.065
39. Zhang YZ, Zhou B, Zhang XP, Huang P, Li CH, Liu Y (2009) Interaction of malachite green with bovine serum albumin: determination of the binding mechanism and binding site by spectroscopic methods. J Hazard Mater 163:1345–1352. doi:10.1016/j.jhazmat.2008.07.132
40. Xiao Q, Huang S, Liu Y, Tian FF, Zhu JC (2009) Thermodynamics, conformation and active sites of the binding of Zn–Nd hetero-bimetallic Schiff base to bovine serum albumin. J Fluoresc 19:317–326. doi:10.1007/s10895-008-0418-y
41. Zhang YZ, Xiang X, Mei P, Dai J, Zhang LL, Liu Y (2009) Spectroscopic studies on the interaction of Congo Red with bovine serum albumin. Spectrochim Acta A 72:907–914. doi:10.1016/j.saa.2008.12.007
42. Tian JN, Liu JQ, Hu ZD, Chen XG (2005) Interaction of wogonin with bovine serum albumin. Bioorg Med Chem 13:4124–4129. doi:10.1016/j.bmc.2005.02.065